PNAS RESEARCH ARTICLE | IMMUNOLOGY AND INFLAMMATION

High-throughput screen identifies non inflammatory small molecule inducers of trained immunity

Hannah Riley Knight[a], Ellen Ketter[b], Trevor Ung[a], Adam Weiss[a], Jainu Ajit[a], Qing Chen[a], Jingjing Shen[a], Ka Man Ip[b], Chun-yi Chiang[b], Luis Barreiro[b], and Aaron Esser-Kahn[a,1]

Edited by Ning Jiang, University of Texas at Austin, Austin, TX; received January 9, 2024; accepted May 29, 2024 by Editorial Board Member Katherine A. Fitzgerald

Trained immunity is characterized by epigenetic and metabolic reprogramming in response to specific stimuli. This rewiring can result in increased cytokine and effector responses to pathogenic challenges, providing nonspecific protection against disease. It may also improve immune responses to established immunotherapeutics and vaccines. Despite its promise for next-generation therapeutic design, most current understanding and experimentation is conducted with complex and heterogeneous biologically derived molecules, such as β-glucan or the Bacillus Calmette-Guérin (BCG) vaccine. This limited collection of training compounds also limits the study of the genes most involved in training responses as each molecule has both training and nontraining effects. Small molecules with tunable pharmacokinetics and delivery modalities would both assist in the study of trained immunity and its future applications. To identify small molecule inducers of trained immunity, we screened a library of 2,000 drugs and drug-like compounds. Identification of well-defined compounds can improve our understanding of innate immune memory and broaden the scope of its clinical applications. We identified over two dozen small molecules in several chemical classes that induce a training phenotype in the absence of initial immune activation—a current limitation of reported inducers of training. A surprising result was the identification of glucocorticoids, traditionally considered immunosuppressive, providing an unprecedented link between glucocorticoids and trained innate immunity. We chose seven of these top candidates to characterize and establish training activity in vivo. In this work, we expand the number of compounds known to induce trained immunity, creating alternative avenues for studying and applying innate immune training.

trained immunity | innate immune memory | inflammation | metabolism | macrophages

Significance

Our work expands the scope of trained immunity for its future study in prophylactic and therapeutic applications, while providing further insights into training pathways. Few molecules induce trained immunity; we report the identification of dozens of small molecule inducers of trained immunity identified through high-throughput screening. The result included compounds with known anti-inflammatory properties. We report a surprising finding that glucocorticoids, traditionally regarded as immunosuppressive, can induce trained immunity.

Trained immunity is described as a nonspecific form of innate immune memory triggered by specific stimuli (1). It is primarily characterized by metabolic and epigenetic rewiring of innate immune cells that amplifies the subsequent response to inflammatory challenges (2). Pathogens or pathogen-derived stimuli like BCG and β-glucan are used as model inducers of trained immunity (3–5). Both of these model training inducers act through pattern recognition receptors (6, 7). Previous work also linked the role of certain endogenous metabolic or hormone molecules, such as aldosterone and oxidized low-density lipoprotein (ox-LDL), to trained immunity (8–11). Each of these inducers of trained immunity reprograms metabolism and chromatin accessibility in conjunction with a primary immune response (as in BCG) or hyperinflammatory disease state. However, this correlation is not causative. It has yet to be demonstrated whether initial immune activation is required for induction of training. Recently, our lab identified a small molecule inducer of trained immunity, A1155463, that is neither pathogen derived nor disease associated (12). Having identified one synthetic training compound, we sought to identify additional small molecule inducers of trained immunity using a high-throughput screening approach. Such a screen would allow us to identify common phenotypes associated with training and identify safe, effective training compounds with possible therapeutic potential.

Many groups have used high-throughput screening to identify small molecule drugs that influence cellular metabolism and epigenetic regulation (13–16). This evidence supported our hypothesis that a screen could successfully identify trained immunity inducers, which often modulate both metabolism and epigenetic pathways (1, 2, 17). Here, we show a high-throughput screen for identifying small molecule inducers of trained immunity. We found over two dozen small molecules that induce trained immunity phenotypes in vitro. We confirmed the in vivo training capacity of seven of the most promising compounds. To determine the potential degree of commonality in their training response, we assessed chromatin accessibility via assay for transposase-accessible chromatin (ATAC)

Author affiliations: [a]Pritzker School of Molecular Engineering, University of Chicago, Chicago, IL 60637; and [b]Biological Sciences Division, University of Chicago, Chicago, IL 60637

Author contributions: H.R.K., L.B., and A.E.-K. designed research; H.R.K., E.K., T.U., A.W., J.A., Q.C., J.S., K.M.I., and C.-y.C. performed research; H.R.K., E.K., L.B., and A.E.-K. analyzed data; and H.R.K., E.K., L.B., and A.E.-K. wrote the paper.

Competing interest statement: H.R.K., J.A., and A.E.-K. are inventors on a patent application for the University of Chicago. The other authors declare no competing interests.

This article is a PNAS Direct Submission. N.J. is a guest editor invited by the Editorial Board.

[1]To whom correspondence may be addressed. Email: aesserkahn@uchicago.edu.

This article contains supporting information online at https://www.pnas.org/lookup/suppl/doi:10.1073/pnas.2400413121/-/DCSupplemental.

Published July 8, 2024.

sequencing on bone marrow-derived macrophages (BMDMs) trained with these hit compounds. Several of these molecules are distinct from known inducers of trained immunity in that they do not induce acute cytokine responses upon initial administration and are not derived from pathogenic or physiologic sources. Additionally, a large proportion of the hit compounds are glucocorticoids, indicating that these drugs may not be limited to their immunosuppressive effects. Through flow cytometric characterization and ATAC-seq, we identified distinct trained phenotypes generated by different inducers of trained immunity. By expanding the number of compounds known to induce training, our work brings trained immunity one step closer to its many potential therapeutic applications (18).

Results

A Screen Identifies Small Molecule Inducers of Trained Immunity. To screen for trained immunity, we had to overcome several challenges of current screening approaches. Screening studies usually probe the activity of compounds against a single protein target rather than a broader phenotypic response, as is required to measure trained immunity. Additionally, most screens require cells to survive for only 1 d and employ immortalized cell lines (16, 19). To determine trained immunity, a typical assay lasts 7 d to allow induction of training, and it requires primary mouse BMDMs, adding additional challenges to the screen (20). The full screening protocol is represented in Fig. 1*A*. The primary readout for a "trained phenotype" response was a fold increase in tumor necrosis factor alpha (TNF-α) on Day 7 relative to cells that did not receive a compound, which served as our "untrained" controls. Our previous experience with high-throughput screening to identify immunomodulators provided insight into the required points of optimization (21). To compensate for challenges with primary cell viability and differentiation, we used several quality control tests during the screening assay to ensure the accuracy and consistency of the experiment across replicates. To ensure the BMDMs were capable of training and the protocol produced consistent results, an additional, identical plate of BMDMs was benchmarked with a standard concentration of 100 μg/mL of β-glucan (20). On Day 5, cell viability was quantified using an IncuCyte and compared to untrained controls (*SI Appendix*, Fig. S1*A*) (22). Trained immunity effects are distinct from innate immune priming, so we checked that the cells maintained a resting phenotype before toll-like receptor (TLR) stimulation by collecting and freezing the supernatant from each of the three screening replicates on Day 6 to measure TNF-α concentration after the assay was complete (*SI Appendix*, Fig. S1*B*). With these technical and biological controls providing reproducible confirmation of training with β-glucan, we applied this screening methodology to identify compounds that could induce a phenotype matching that produced by β-glucan, analogous to training, in vitro.

After optimization, we proceeded to screen 2,000 small molecules from the MicroSource Spectrum Library. For each replicate of the screen, a modified version of the standard 7-d training assay was used (20). TNF-α concentration was measured using a Quanti-Blue assay in human embryonic kidney (HEK)-Blue TNF-α cells. To test TNF-α concentration in the supernatant, HEK-Blue TNF-α cells were plated at 25,000 cells per well in 384-well plates with 5 μL of the supernatant. The cells were incubated with the supernatant for 24 h before 20 μL of concentrated QuantiBlue reagent was added to the plate. After 15 min, the absorbance was measured at 628 nm. We defined a hit as exhibiting a 1.6-fold or greater increase in TNF-α production over stimulated, untrained controls. We selected this cutoff as it is 2.5 SD from the mean of all library compounds. During screening optimization, β-glucan exhibited a 1.7-fold increase in TNF-α production over untrained controls, which was consistent with our previous work (*SI Appendix*, Fig. S1*C*) (23). We chose a slightly lower cutoff for hit validation, as the initial library concentration of 1 μM may not have been optimal for every compound tested. Thirty-two compounds exceeded the 1.6-fold increase threshold, representing 1.5% of the compounds tested (Fig. 1*B*). These compounds had several common characteristics, and so we classified them into seven groupings.

Glucocorticoids made up 13 of the top 24 compounds. While one endogenous mineralocorticoid has been shown to induce trained immunity, the induction of innate immune training by glucocorticoids was both unique and surprising. However, there is literature precedence for the complicated effects produced by glucocorticoids in innate immune cells (24, 25). Interestingly, in an examination of the literature, one study from 1993 determined that synthetic hypercortisolemia in humans initiated 6 d before endotoxin (LPS) challenge resulted in elevated serum cytokine levels, though no possible cause was indicated (26). We hypothesize that trained immunity may help explain this observation. The remaining hit compounds consisted of adrenergic agonists, pesticides, and antineoplastic drugs (Fig. 1*C*). To capture a broad range of possible training pathways, we selected seven top-performing compounds (including representative compounds from each classification) for further investigation in vitro and in vivo (Fig. 1 *D* and *E*).

Nonimmunogenic Small Molecules Suppress Acute Inflammation but Induce a Training Phenotype in a Dose-Dependent Manner. Having identified a set of compounds that increased TNF-α secretion after TLR stimulation, we wanted to validate whether they have similar training activity to other known training agents through further in vitro study. To ensure that we chose the optimal concentration and agonist pairing, we first conducted a series of enzyme-linked immunosorbent assays (ELISAs) to validate the training effects. A total of 100,000 BMDMs per well were plated in 96-well plates on Day 0. On Day 1, BMDMs were trained with hit compounds at multiple concentrations (100 nM to 10 μM) to identify the most effective concentration without inducing toxicity (Fig. 2*A*). The remainder of the assay proceeded as previously described, and the supernatant was collected on Day 7. TNF-α concentration in the supernatant was measured using ELISAs. Most compounds elicited a significant, positive dose-dependent training response, and 10 μM was the most effective at inducing upregulation of TNF-α across most hit compounds (*SI Appendix*, Fig. S2*B*). Therefore, 10 μM was selected for all subsequent in vitro experiments. It is possible that cytotoxicity at even higher concentrations could dampen the effects of training in vitro. In each experiment, the elevation of both TNF-α and interleukin-6 (IL-6) was observed in BMDMs trained with the seven compounds (*SI Appendix*, Fig. S2*A*). A hallmark of trained immunity is an increased cytokine response to heterogeneous challenges, contributing to its ability to provide broad protection against multiple pathogens (24). To demonstrate that effective training responses are compatible with multiple TLR agonists, BMDMs trained with hydrocortisone were stimulated with either LPS (TLR4 agonist) or Pam3CSK4 (TLR1/2 agonist) (Fig. 2*B*). With each TLR agonist, the trained BMDMs exhibited about 30% increased TNF-α production over untrained BMDMs.

We were interested in identifying similarities and differences between our hit compounds and known training compounds. Unlike β-glucan and BCG, these hit compounds do not induce proinflammatory cytokine production within the first 24-h window of incubation with BMDMs. (*SI Appendix*, Fig. S2*C*). In fact, some compounds significantly suppress acute inflammation when given 1 h before stimulation with LPS (Fig. 2*C*). We also collected

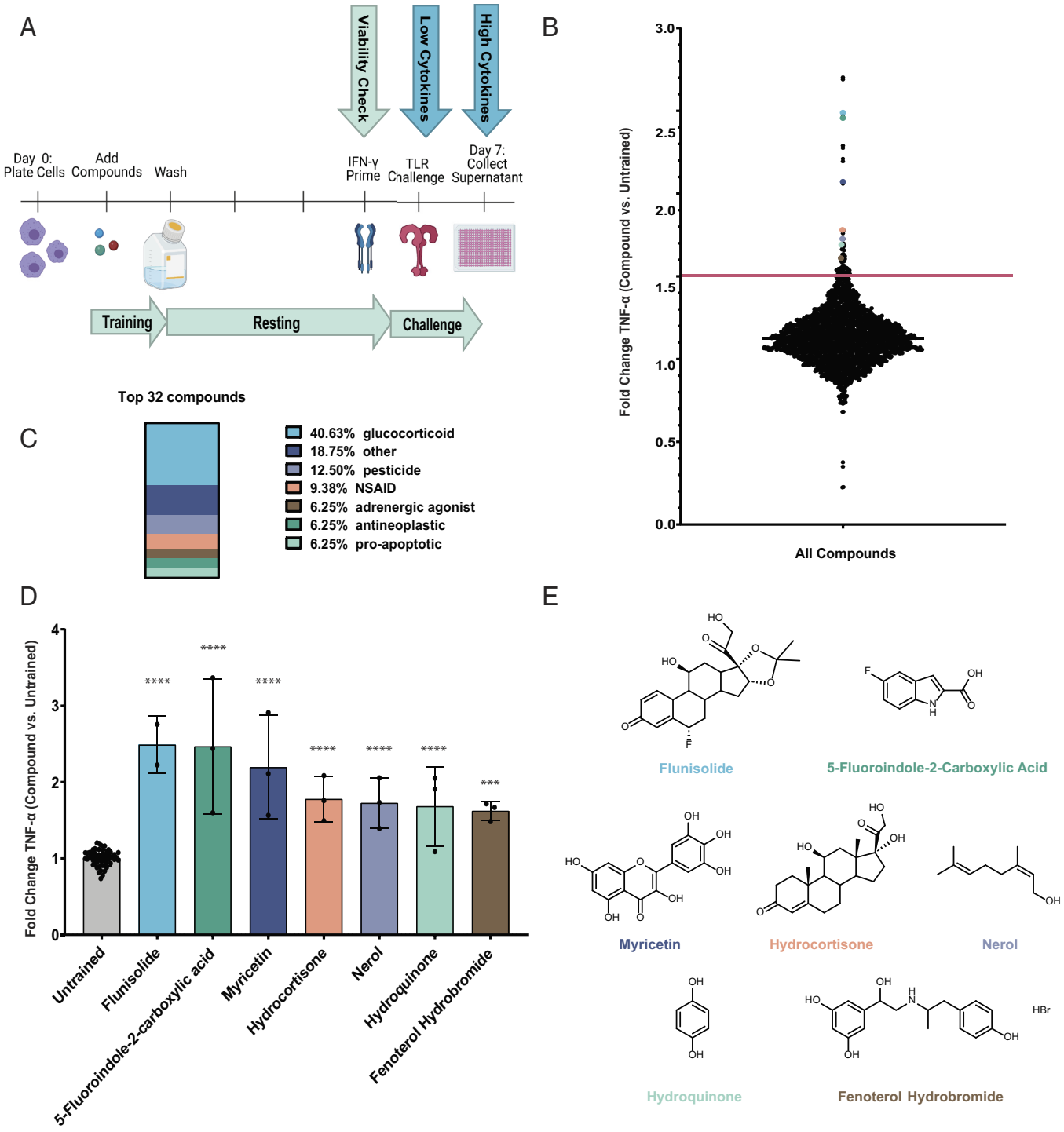

Fig. 1. High-throughput screen for small molecule inducers of trained immunity identified seven lead compounds. (*A*) Schematic of high-throughput screen design and checkpoint measurements. (*B*) All compounds' TNF-α concentration represented as fold change over untrained control (n = 3). The pink line at fold change = 1.6 represents the cutoff for hit identification. (*C*) Classification by previously identified activity of 32 hit compounds represented as a percent of the total. (*D*) Seven hit compounds chosen for further evaluation represented as TNF-α concentration fold change over untrained control ranging from 1.6-fold to 2.5-fold increase. (*E*) Chemical structure of seven hit compounds. All values are expressed as mean ± SEM, and statistics were conducted using one-way ANOVA with Dunnett's multiple comparisons test (significance compared with untrained group ***$P < 0.001$ and ****$P < 0.0001$. See also *SI Appendix*, Fig. S1.

the supernatant on Day 6 immediately prior to TLR stimulation. The supernatant collected on Day 6 displayed negligible proinflammatory cytokine production, suggesting that the response is not dependent on cytokine activation of innate cells. (*SI Appendix*, Fig. S2*D*). In contrast to known inducers of training, these compounds were unique in their inflammatory signatures, so we sought to discern potential pathway involvement of known metabolic and epigenetic characteristics.

Glucocorticoid Training Is Dependent on Glycolysis. Upregulation of glycolysis is commonly implicated as one of the underlying mechanisms in the induction of trained immunity (7). We tested representative top-performing compounds using a standard glycolytic inhibitor of training given 1 h before small molecule administration (20, 27). A reduction in cytokine elevation compared to untrained controls would indicate glycolytic involvement. In our glucocorticoids, flunisolide and hydrocortisone, we observed

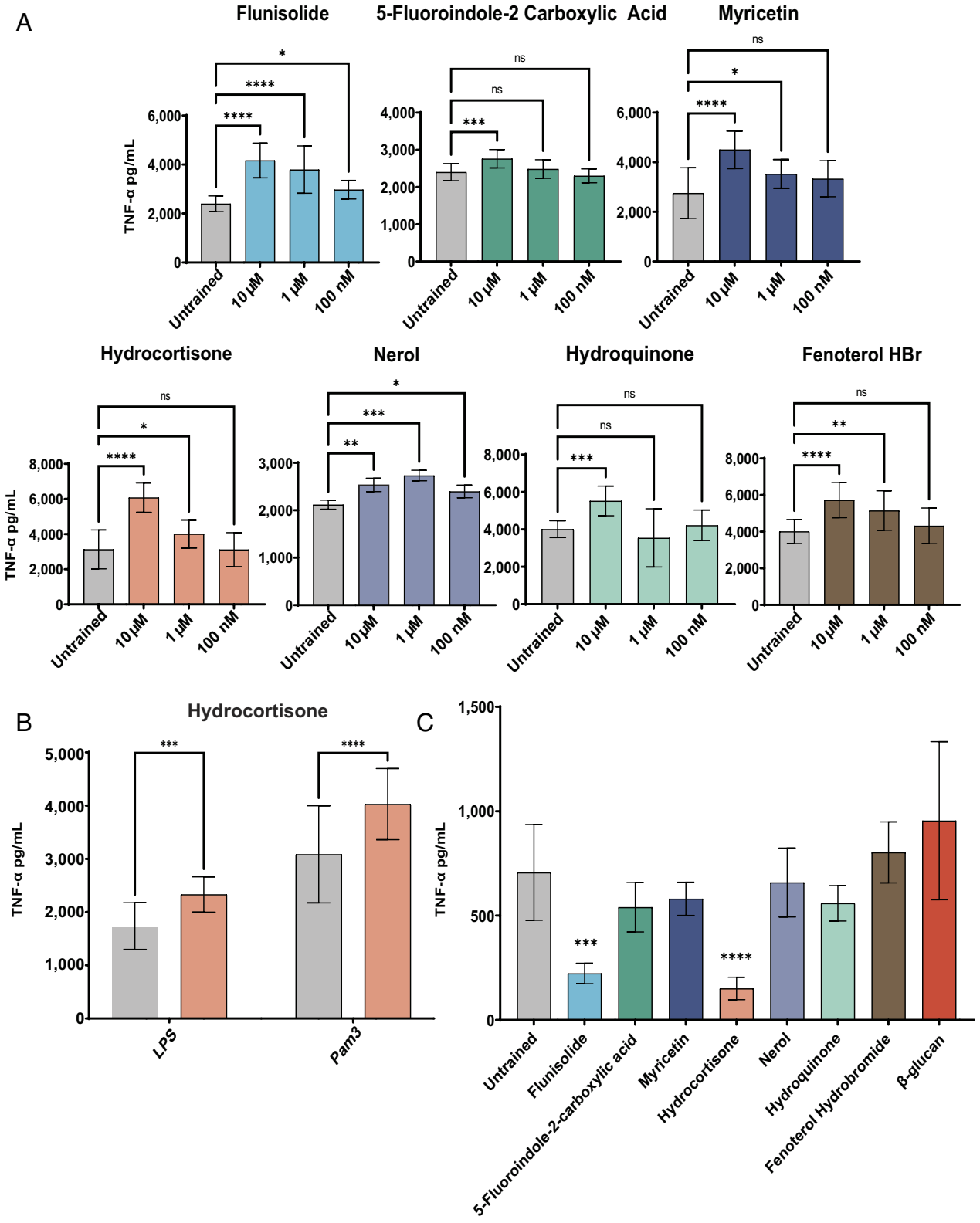

Fig. 2. In vitro confirmation of screen hits. (*A*) TNF-α concentration from BMDMs trained with phosphate-buffered saline (PBS) or hit compounds at a concentration of 10 μM to 100 nM followed by a challenge with 100 ng/mL Pam3 (n = 15).The most effective concentration for subsequent in vitro experiments was determined to be 10 μM. (*B*) TNF-α concentration from BMDMs trained with PBS or hydrocortisone at a concentration of 10 μM followed by challenge with 100 ng/mL LPS or Pam3 (n = 30). Training effects were observed with both TLR4 and TLR1/2 agonists. (*C*) Test of preliminary anti-inflammatory response of compounds. TNF-α or IL-6 concentration from BMDMs treated with 10 μM hit compounds 1 h prior to 24 h stimulation with 100 ng/mL LPS (n = 6). In an acute (nontraining) LPS challenge, glucocorticoids significantly suppressed TNF-α production. All values are expressed as mean ± SEM, and statistics were conducted using one-way or two-way ANOVA with multiple comparisons (significance compared with untrained group). *$P < 0.05$, **$P < 0.01$, ***$P < 0.001$, ****$P < 0.0001$, and n.s., not significant. See also *SI Appendix*, Fig. S2.

significant inhibition of training in response to glycolysis inhibition (2-deoxy-D-glucose) (Fig. 3*A*). However, all other compounds besides glucocorticoids did not respond to inhibition of the glycolytic training pathway in the assay (Fig. 3*B*). The untrained control did not respond to treatment with inhibitors, as expected. Furthermore, flunisolide was significantly responsive to inhibition with 5′-deoxy-5′-(methylthio)adenosine (MTA), a histone methyltransferase inhibitor, but was not significantly inhibited by (–)-epigallocatechin-3-gallate (EGCG), a histone acetylase inhibitor (*SI Appendix*, Fig. S3). These results suggest that glucocorticoids induce trained immunity through glycolytic and epigenetic pathways and that different pathways may be involved in training with other compounds.

ATAC-seq Reveals Differential Chromatin Accessibility between Small Molecule-Trained BMDMs. We posited that training with distinct small molecules would induce alterations in chromatin accessibility, and these changes could potentially vary depending on the specific stimulus from each training compound. To evaluate this hypothesis, we isolated nuclei from BMDMs 4 d after their exposure to the top seven hit compounds and conducted ATAC-seq experiments (Fig. 4*A*). Subsequently, we identified regions of open chromatin peaks that exhibited significant alterations in accessibility levels in response to the diverse treatments. To enhance statistical power and precision in estimating effect sizes for these "Differentially Accessible (DA) peaks", we employed a multivariate adaptive shrinkage method known as "mash", which capitalizes on the correlation structure of effect sizes across the various treatments (28).

The greatest number of DA peaks was observed in macrophages treated with β-glucan [comprising 36,235 peaks classified as DA at a false discovery rate (FDR) = 5%], followed by flunisolide (n = 11,683 DA peaks) (Fig. 4*B* and *SI Appendix*, Fig. S4*A*). Conversely, all other treatments resulted in a lower number of DA peaks, with the fewest changes being observed in response to Hydroquinone (n = 7,316 DA peaks). A correlation analysis

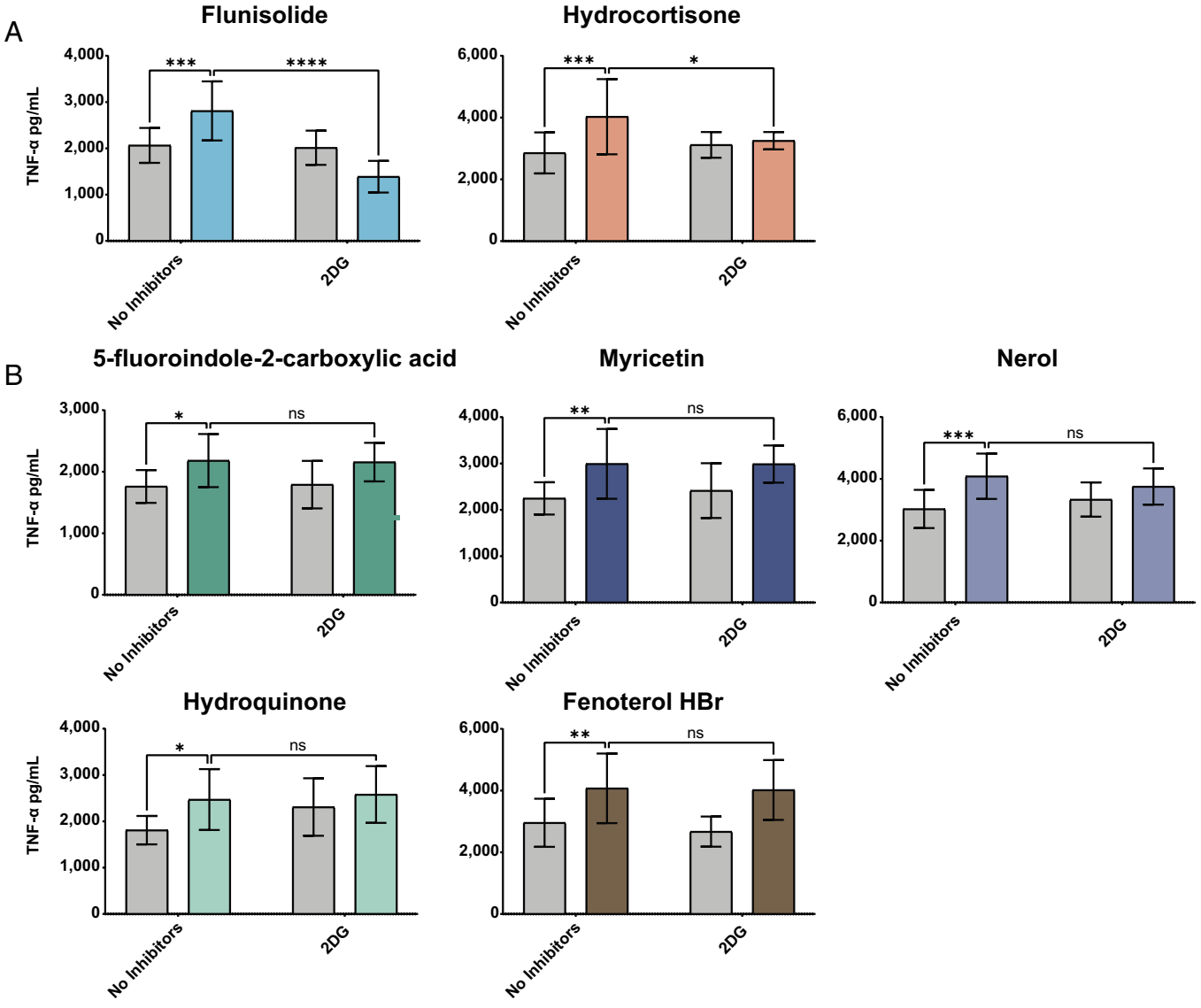

Fig. 3. Chemical inhibition of trained immunity results in response from some compounds. (*A*) Glycolysis inhibition assay using 1 mM 2-Deoxy-D-Glucose (2DG) and measuring TNF-α concentration following Pam3 challenge in cells trained with 10 μM flunisolide or hydrocortisone after 1 h of pretreatment with PBS or 2DG (n = 15). Inhibition of metabolic pathways prevents induction of training via glucocorticoids. (*B*) TNF-α concentration following Pam3 challenge in cells trained with 10 μM 5-fluoroindole-2-carboxylic acid, myricetin, nerol, hydroquinone, or fenoterol hydrobromide after pretreatment with PBS or glycolysis inhibitor, 2DG (n = 15). These small molecules were not susceptible to suppression of training via inhibition of glycolysis. All values are expressed as mean ± SEM, and statistics were conducted using two-way ANOVA with Sidak's multiple comparisons test (significance compared with untrained group). **P* < 0.05, ***P* < 0.01, ****P* < 0.001, *****P* < 0.0001, and n.s., not significant. See also *SI Appendix*, Fig. S3.

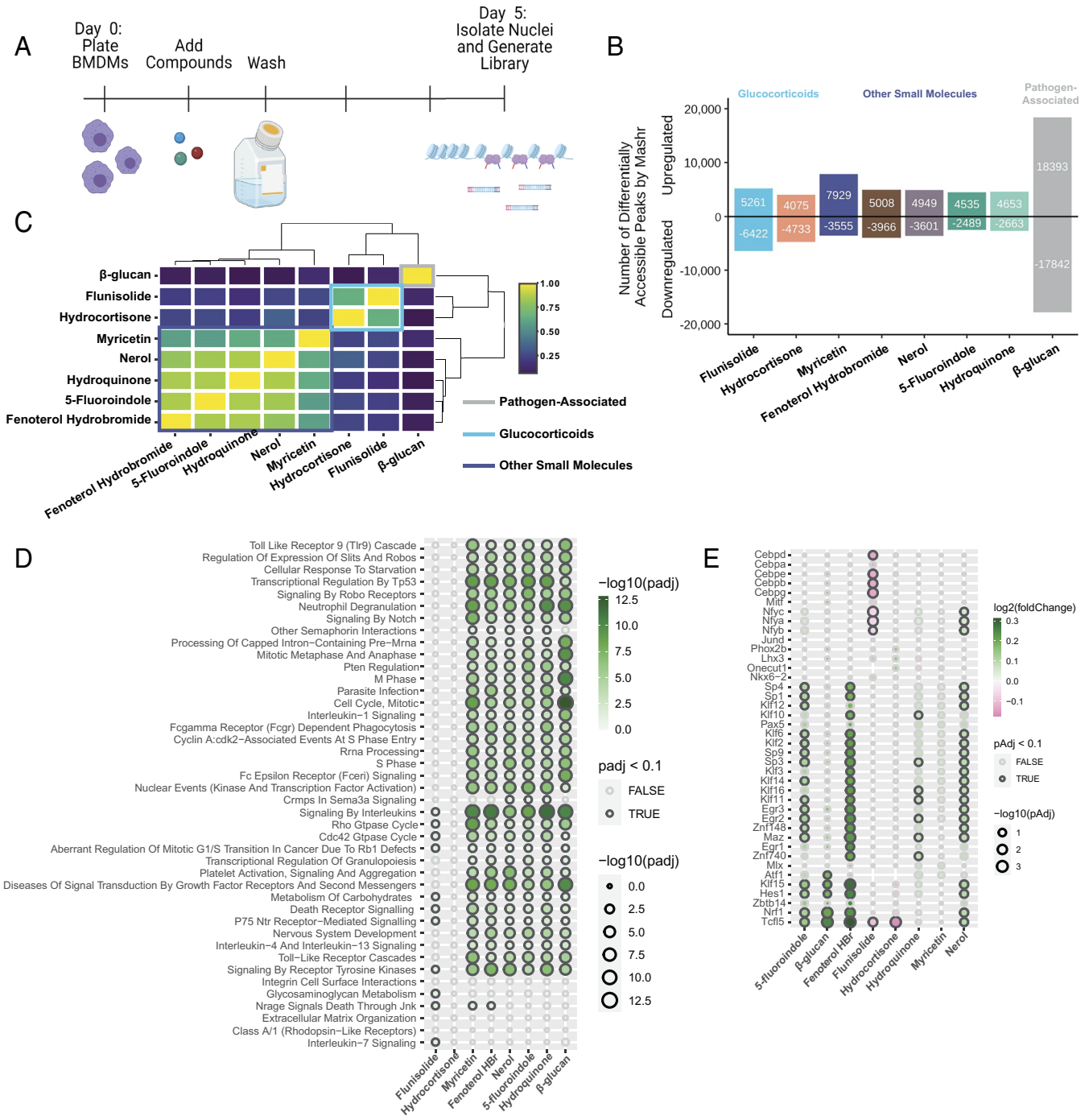

Fig. 4. ATAC-seq identifies unique chromatin regulation in glucocorticoid-trained BMDMs. (*A*) Schematic of BMDM training protocol for ATAC-seq library preparation. (*B*) Plot demonstrating the number of peaks with increased or decreased accessibility compared to untreated controls (LFSR < 0.05). (*C*) Independent clustering of shared differentially accessible peaks by treatment shows that glucocorticoids share a unique profile compared to β-glucan or other small molecule-trained BMDMs. (*D*) Two-list enrichment analysis identifies differentially accessible pathways shared between BMDMs trained by different stimuli. (*E*) TF footprints show increased binding of KLF and Sp family transcription factors in β-glucan and nonglucocorticoid small molecule-trained BMDMs. Glucocorticoid-trained BMDMs also exhibited decreased CEBP TF binding. See also *SI Appendix*, Fig. S4 and Datasets S1–S3.

of effect sizes across treatments revealed three distinct clusters: Cluster 1 encompassed β-glucan, cluster 2 included glucocorticoids, while cluster 3 incorporated all remaining treatments (Fig. 4*C* and *SI Appendix*, Fig. S4*B*). This observation indicates that the pattern of chromatin alterations linked to functional training diverges based on the specific stimulus. Our analysis of differential accessibility unveiled distinct epigenetic signatures unique to glucocorticoids, pathogen-associated β-glucan, and training with other small molecules.

To further understand how these compounds influence transcriptional response, we examined genes with the greatest accessibility both for individual molecules and for those commonly shared across all compounds including β-glucan. These commonly shared alterations in chromatin accessibility are presented in *SI Appendix*, Fig. S4*C*. Two of the most statistically significant peaks for which chromatin accessibility increased among all compounds tested localized near SH3GLB1 and SCARB1 transcription start sites (Dataset S1). SH3GLB1 affects mitochondrial dynamics, autophagy, and

apoptosis, and SCARB1 is a scavenger receptor involved in cholesterol uptake and metabolism (29, 30). Gene set over-enrichment analysis identified a significant increase in chromatin openness (FDR = 10%) nearby genes in several pathways thought to be important for trained immunity in each of the treatments tested. Such pathways include interleukin signaling, TLR signaling, phagocytosis, chromatin modification, and carbohydrate metabolism (Fig. 4*D* and Dataset S2). When analyzing only the peaks that changed accessibility levels across all treatments, we found an enrichment of accessibility nearby genes related to IL-4 and IL-13 signaling pathways and transcriptional regulation of granulopoiesis (*SI Appendix*, Fig. S4*C*). Interestingly, we found a specific enrichment of G-protein coupled receptor (GPCR) ligand binding, and rhodopsin-like receptor activity (*SI Appendix*, Fig. S4*C*) in glucocorticoid-trained BMDMs. This result implies that glucocorticoids induce changes that are distinct from common training pathways.

We next aimed to understand what transcription factors (TFs) might be associated with the observed changes in the epigenetic landscape of BMDMs treated with the different molecules. Across all treatments, NF-κB, Jun, Fos, and CEBP binding sites were enriched among regions that gained chromatin accessibility, suggesting that the activation of these TFs in response to the different treatments is likely a driving force behind the epigenetic changes identified (*SI Appendix*, Fig. S4*F*). Previous work in trained immunity has identified Jun and Fos as key transcriptional regulators of training (31). Additionally, we noticed increased motif enrichment of Krüppel-like factors (KLF) and Specificity protein (Sp) family TFs, which are associated with cell proliferation and differentiation, in all treatments except for the glucocorticoids (32). Notably, KLF14, enriched in each of the nonsteroid treatments, has been shown to regulate glycolysis in macrophages (33). We then performed footprinting analysis to determine whether there were differences in bound TFs between the training molecules in the trained, unstimulated state. While this will not determine how TFs behave in trained cells responding to inflammatory challenge, it may provide insights into the roles of TFs in the induction of the trained state. There was a decrease in actively bound TFs in glucocorticoid-trained BMDMs, whereas training with the other small molecules or β-glucan increased the number of bound TFs relative to PBS-treated BMDMs (*SI Appendix*, Fig. S4*D*). Many of the KLF and Sp family TFs were identified in footprinting analysis and share consensus motifs (Dataset S3), though many of these TFs compete for the same binding sites and have both repressor and activator functions (Fig. 4*E* and *SI Appendix*, Fig. S4*E*) (34). Unsurprisingly, neither NF-κB nor its subunits showed evidence of occupancy in the footprinting analysis, emphasizing that the trained, unstimulated BMDMs do not promote constitutive inflammatory activation (*SI Appendix*, Fig. S4*E*). These findings collectively suggest that training with distinct small molecules can induce both the fundamental chromatin remodeling necessary for initiating training across all treatments and distinctive epigenetic changes likely mediated by the activation of distinct sets of TFs as implied by the footprinting analysis. The unique patterns of activation of trained immunity demonstrated by the glucocorticoids and other small molecule inducers of training deserve further mechanistic study.

Non Inflammatory Small Molecules Induce Trained Immunity Responses In Vivo. Next, we sought to determine whether the small molecules we identified and validated in vitro could induce training responses in vivo. To test this question, three training injections were given intraperitoneally (IP) to 6-wk-old female C57Bl/6 J mice every other day. Each compound was formulated in 50 μL injections solubilized in 10% dimethyl sulfoxide (DMSO) and 90% corn oil. Hydrocortisone and 5-fluoroindole-2-carboxylic acid were given at a dose of 2 μmol per injection, as they were less potent than the remaining compounds, which were given at a dose of 1.5 μmol per injection. For the untrained control, mice received only the carrier solution with no added compound. After a 7-d rest period, mice were challenged with 1 μg LPS IP (Fig. 5*A*). Serum was collected via the submandibular vein 1 h after challenge and tested for the proinflammatory cytokines TNF-α and IL-6 using ELISAs. Compared to the untrained control, each of our seven selected compounds exhibited elevated TNF-α and IL-6 serum cytokines, ranging from 1.6-fold increase in cytokine production for fenoterol hydrobromide to fourfold increase for flunisolide (Fig. 5*B*). This difference suggests that training with our small molecule hits substantially increased innate immune response to inflammatory challenge.

We wanted to determine the cells and cell types that were contributing to the increase in serum cytokines from training with our small molecules. We selected three of the most promising compounds, flunisolide, myricetin, and hydroquinone, to investigate the cellular response. To determine which cells were involved, mice were given training injections and challenged as previously described. Then, 2 h after challenge, the mice were killed, and peritoneal cells were collected by lavage. The cells were fixed and stained for intracellular TNF-α and IL-6 and surface costimulatory markers, CD40, CD86, and MHCII. We also included lineage markers for innate immune cells, including neutrophils, eosinophils, monocytes, macrophages, and dendritic cells. The stained cells were then analyzed via spectral flow cytometry. We initially observed that mice trained with flunisolide or myricetin exhibited increased cell count in the peritoneal lavage when compared to untrained or β-glucan trained controls (Fig. 5*C*) The increases in cell numbers were distinctive for each training compound. Flunisolide- and myricetin-trained mice exhibited significant increases in the number of TNF-α^+ and IL-6^+ eosinophils (Fig. 5*D*). Mice trained with hydroquinone presented a different phenotype. While there was no increase in the number of TNF-α^+ and IL-6^+ cells, there were significant increases in the cytokine median fluorescence intensities (MFIs) among TNF-α^+ neutrophils and IL-6^+ eosinophils in the hydroquinone-trained mice (Fig. 5*E*). These results suggest that flunisolide and myricetin promote a stronger production of TNF-α and IL-6 via the increased number of eosinophils generating these cytokines. Alternatively, hydroquinone induces greater production of TNF-α and IL-6 in neutrophils, but not significantly greater number. This contrasts with β-glucan which does not generate a greater number of cells in the peritoneal space but still resulted in higher MFI of IL-6 in eosinophils.

We also considered how activation of these cells resulted in changes to costimulatory molecules. When considering stimulatory surface molecules such as CD86 and MHCII, only flunisolide-trained mice were significantly different from controls. Flunisolide-trained mice exhibited an increased amount of CD86 on eosinophils and small peritoneal macrophages (SPMs), as measured by MFI of CD86$^+$ cells (Fig. 5*F*). Additionally, the MFI of MHCII$^+$ SPMs was also increased in mice trained with flunisolide (Fig. 5*G*). β-glucan-trained mice exhibited increased MFI of MHCII$^+$ eosinophils, neutrophils, and large peritoneal macrophages (LPMs). Taken together, these data indicate that while there are similar increases in serum cytokines in small molecule-trained mice, there are differences in the cellular profile of the innate cells that respond to LPS challenge dependent on the training molecule. Thus, there may be differences in the cellular mechanisms by which each small molecule induces trained immunity in vivo.

Discussion

Trained immunity can improve immune responses to pathogens, cancer, vaccination, and prophylaxis (23, 35–37). However, few molecules are known to induce training, and the existing repertoire of compounds is limited (38–40). Expanding the number of known

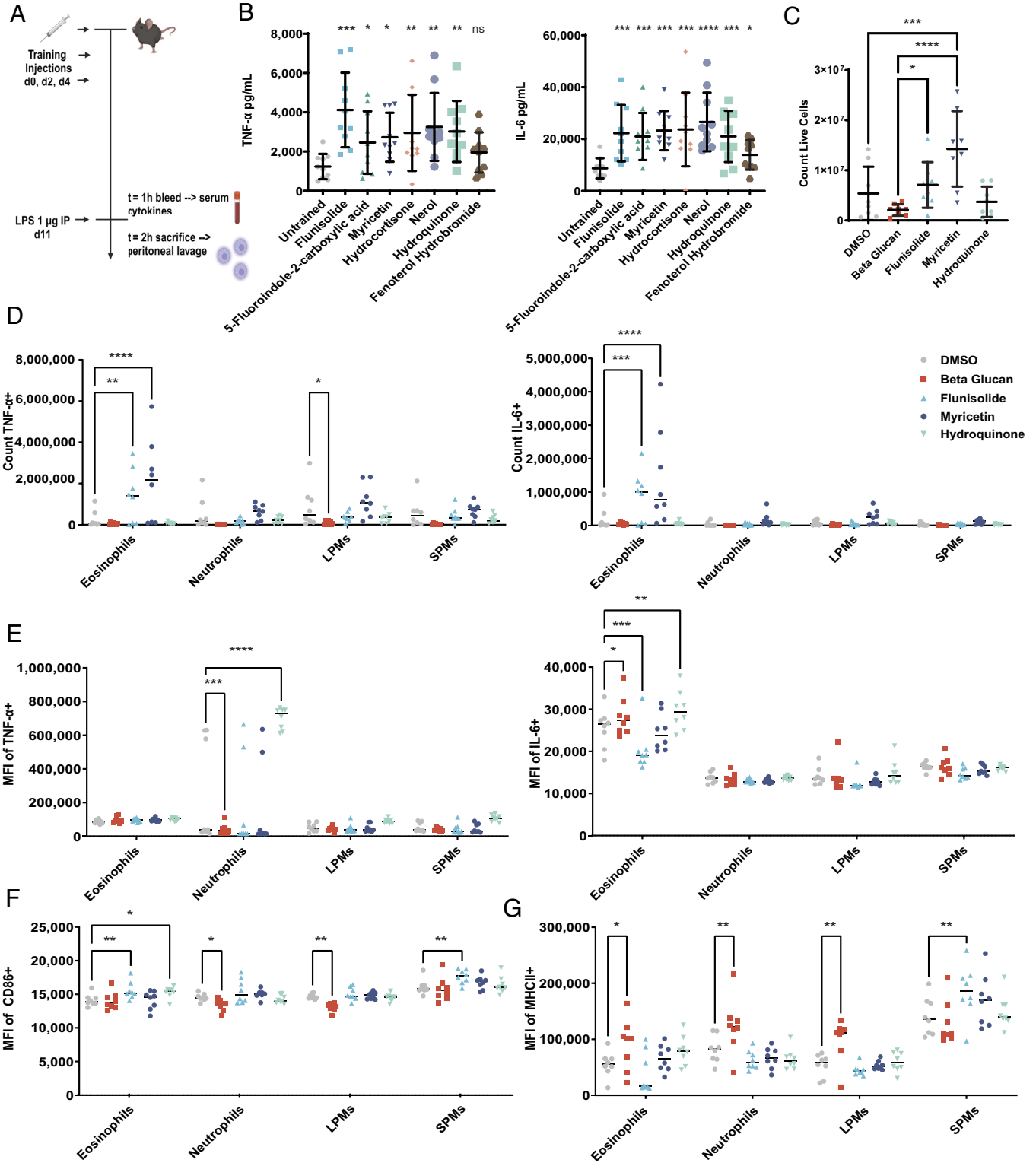

Fig. 5. In vivo training with small molecules shows differences in cellular response. (*A*) Schematic of small molecule training in vivo. Mice were injected IP with small molecules or vehicle control on Days 0, 2, and 4. Mice were challenged with 1 µg LPS on Day 11 and then bled 1 h later or killed 2 h later followed by peritoneal lavage. (*B*) TNF-α or IL-6 concentration from mice trained with vehicle or small molecule inducers of training (n = 10). Hydrocortisone and 5-fluoroindole-2-carboxylic acid were dosed at 2 µmol, and the remaining compounds were dosed at 1.5 µmol. For each hit compound, increased proinflammatory cytokine responses were observed at 1 h. (*C*) Mice trained with myricetin exhibited significantly increased cell count in the peritoneal cavity 2 h after challenge. (n = 8). (*D*) Training with either flunisolide or myricetin resulted in a significantly increased number of IL-6$^+$ or TNF-α$^+$ eosinophils in the peritoneal lavage. (*E*) Training with hydroquinone resulted in significantly higher MFI of TNF-α$^+$ neutrophils and IL-6$^+$ eosinophils in the peritoneal lavage. (*F*) Mice trained with flunisolide had a significant increase in MFI of CD86$^+$ eosinophils and SPMs. (*G*) Mice trained with flunisolide had a significant increase in MFI of MHCII$^+$ SPMs. B-glucan trained mice had significant increase in MFI of MHCII$^+$ eosinophils, neutrophils, and LPMs. All values are expressed as mean ± SEM, and statistics were conducted using one-way ANOVA or two-way ANOVA with multiple comparisons (significance compared with untrained group). *$P < 0.05$, **$P < 0.01$, ***$P < 0.001$, ****$P < 0.0001$, and n.s., not significant.

inducers of trained immunity, each with unique properties, can improve our ability to control this immunological process for therapeutic applications (41, 42). Here, we report a high-throughput screen to identify molecules that induce trained immunity responses, thus rapidly expanding the number of non inflammatory inducers of training available. Furthermore, many of these small molecules are pharmaceuticals currently available in a variety of formulations and are approved by the Food and Drug Administration (FDA) at higher doses for the treatments of other immunological responses. The ease of manufacture and delivery of these drugs supports the potential for trained immunity to be used as a clinical strategy for both disease prevention and treatment. Further investigation into their use in training may be warranted given these promising conditions.

We identified 32 and further characterized seven nonimmunogenic small molecule inducers of trained immunity that exhibited improved cytokine responses over untrained controls both in vitro and in vivo. This library of training compounds, spanning diverse classes of drugs ranging from glucocorticoids to adrenergic compounds and others, allowed us to develop mechanistic insight toward both known and unknown training pathways. We demonstrated the involvement of canonical trained immunity pathways generated by two compounds, flunisolide and hydrocortisone, using glycolytic inhibitors of training. To improve our understanding of these small molecule training pathways, we pursued ATAC-seq to identify differentially accessible genes and TF binding sites compared to untrained controls. These results include signatures induced by the identified training compounds that are both shared with and unique from the previously identified inducers of trained immunity. These shared signatures suggest a common set of binding sites and accessible genes required to induce a trained response in vivo. Of note, the total number of chromatin changes generated by these small molecules is substantially less by about three times (~10,000 versus ~35,000) than those identified for the large, pathogen-associated training compound β-glucan. This implies that the minimal set of epigenetic changes necessary to initiate training may be a much smaller subset of the total number of chromatin changes induced by classical training agents.

In summary, we report on both molecules identified by high-throughput screening and their distinct activity for inducing trained immunity phenotypes. In this report, we have more than doubled the number of molecular entities reported to elicit trained immunity. Moreover, we have identified many compounds that elicit training without eliciting inflammatory responses on their own or which have active repression of inflammation in the first 24 h window. Future studies will be needed to determine the preferred targets for trained immunity for therapeutics, to understand whether small molecules alter the differences in central versus peripheral training, and to establish the therapeutic efficacy of this approach in human disease. We believe that small molecule inducers of training provide innovative tools to identify the answers to these complex problems by expanding potential routes of administration while avoiding unnecessary innate immune activation.

Materials and Methods

Animals. Six-week-old female C57Bl/6 J mice were obtained from Jackson Laboratories and acclimatized for 1 wk before experimentation. All animal experiments were conducted with approval from the University of Chicago Institutional Animal Care and Use Committee (approval number 72517).

Chemicals. The screen was completed using Microsource Spectrum Library purchased through the Cellular Screening Center. Stock compounds for future experiments are listed in the *SI Appendix, Key Resources Table*.

BMDMs. BMDMs were harvested from the femurs of 6-wk-old C57Bl/6 J mice as reported previously (21). They were plated at a density of 50×10^6 cells/10 cm dish in primary culture medium: RPMI 1640 (Life Technologies), 10% heat-inactivated fetal bovine serum (HIFBS), 2×10^{-3} M L-glutamine (Life Technologies), antibiotic antimycotic (1×) (Life Technologies), and 10% MCSF (*Mycoplasma* free L929 supernatant) for 5 d at 37 °C and 5% CO_2. On Day 6 of culture, cells were detached with 5 mM EDTA in PBS, counted, and plated for further assays.

High-Throughput Trained Immunity Screening. Mature BMDMs were plated at 25,000 cells per well in 45 μL media in 384-well flat-bottomed plates using the Thermo Multidrop Combi liquid handler. Cells were rested overnight at 37 °C and 5% CO_2. The following day, training compounds from the Microsource Spectrum Library were added at a volume of 45 nL using the PerkinElmer Janus G3 with Pintools for a final concentration of 1 μM. On Day 2, the supernatant was removed using the Janus, cells were washed with warm PBS using the Multidrop, and fresh medium was added to the cells using the Multidrop. On Day 5, cell density was quantified using the IncuCyte imager and software and then, cells received medium containing 25 ng/mL IFN-γ (BioLegend) for 24 h. On Day 6, cells were stimulated with 25 ng/mL Pam3CSK4 (Invivogen). The supernatant was collected on Day 6 and on Day 7 following 24 h of TLR stimulation, and it was stored at −80 °C.

To measure TNF-α concentration in the supernatant, a high-throughput Quanti-Blue assay was used. HEK-Blue TNF-α cells (Invivogen) were plated at a density of 25,000 cells per well in 45 μL media (DMEM, 10% HIFBS). Five microliters of the supernatant is added to each well using the Janus liquid handler; then, the plates were incubated for 24 h at 37 °C and 5% CO_2. The following day, 20 μL of concentrated Quanti-Blue reagent was added to each well using the Combi liquid handler, and the plate was shaken for 1 min. Then, the plate was incubated at room temperature for 15 min before absorbance was measured at 628 nm using the BioTek Synergy NEO 2. All data are represented as a fold change relative to the average of the Pam3-only untrained control (n = 20) on each plate.

In Vitro Trained Immunity Assay. Mature BMDMs were plated at 10^5 cells per well in 200 μL media in 96-well flat-bottomed plates. Cells were allowed to rest overnight at 37 and 5% CO_2. Following the overnight rest, training molecules were added at specified concentrations and incubated for 24 h. After training, cells were washed with warm PBS and rested for 3 d in fresh media. On Day 5, cells received fresh media containing 25 ng/mL IFN-γ (BioLegend) for 24 h. On Day 6, cells were stimulated with 100 ng/mL Pam3CSK4 (Invivogen). The cell supernatant was collected 24 h after stimulation. Supernatants were measured for IL-6 and TNF-α concentrations using ELISA MAX Deluxe kits (BioLegend) according to the manufacturer's instructions.

For inhibition studies, BMDMs received inhibitors at specified concentrations 1 h prior to stimulation with training molecules, and inhibitors were present for the entire 24 h training period. To test epigenetic pathway involvement, MTA and EGCG were used at final concentrations of 500 μM and 15 μM, respectively. To test metabolic pathway involvement, cells were pretreated with 1 mM 2′ deoxy-D-glucose.

In Vivo Trained Immunity Assay. C57Bl/6 J mice were trained via IP injection. For each compound, mice were treated with 1.5 to 2 μmol of the indicated small molecule in 50 μL (10% DMSO and 90% Corn Oil) every other day for a total of three training injections. Mice were rested for 7 d following the final injection, and then challenged IP with 1 μg LPS (serotype O55:B5; Invivogen) in 100 μL PBS. Mice were bled via the submandibular vein 1 h following LPS injections or killed 2 h following LPS injections. After submandibular bleeds, serum was prepared by allowing the blood to clot for 30 min, then centrifuged for 15 min at 2,000 × g. Serum cytokines were quantified via the ELISA (BioLegend) for IL-6 and TNF-α according to the manufacturer instructions. After the mice were killed, peritoneal lavage was performed with 4 mL cold PBS with 3% HIFBS, and cells remained on ice until preparation for flow cytometry.

Intracellular Cytokine Staining and Flow Cytometry. After sac, peritoneal cells were centrifuged at 500 × g for 5 min and then resuspended in 1 mL ACK lysis buffer to eliminate any red blood cell contamination. After 3 min of ACK lysis, the suspension was diluted to 15 mL in PBS and then centrifuged again. Cells were then resuspended in Improved Minimum Essential Media (IMEM) containing 10% HIFBS, 2×10^{-3} M L-glutamine (Life Technologies), antibiotic antimycotic (1×) (Life Technologies), and GolgiPlug (BD Biosciences) and GolgiStop (BD Biosciences). The cells were counted and plated at a concentration of 1×10^6 cells/well in a 96-well U-bottom plate. The cells were then incubated with GolgiPlug and GolgiStop for a total of 4 h to block cytokine secretion. After incubation, cells were centrifuged and washed

with fluorescence activated cell sorting (FACS) buffer and then incubated with FcBlock and Live/Dead Aqua for 15 min at room temperature. Next, cells were stained for surface antigens for 20 min at room temperature. Cells were then fixed and permeabilized using Cytofix/Cytoperm (BD Biosciences) for 20 min and then stained for intracellular cytokines for 30 min at room temperature. Fixed, stained samples were stored at 4 °C overnight and then analyzed via spectral flow cytometry with the Cytek Aurora.

ATAC-seq Sample Preparation.

Treatment and transposition. Mature BMDMs were plated at 10^5 cells per well in 200 μL media in 96-well flat-bottomed plates (Corning) and rested overnight at 37 °C and 5% CO_2 and then trained. Training molecules were added at specified concentrations in media and incubated for 24 h: 10 μM flunisolide, 10 μM 5-fluoroindole-2-carboxylic acid, 10 μM myricetin, 10 μM hydrocortisone, 10 μM nerol, 10 μM hydroquinone, 10 μM fenoterol hydrobromide, and 100 μg/mL beta glucan. Untrained controls were given media with 20 μL of PBS in place of the training molecules. On Day 5 cells received fresh media without IFN-γ. On Day 6, cells were detached from the plate in lysis buffer [10 mM Tris-HCl, pH 7.4, 10 mM NaCl, 3 mM MgCl2, and 0.1% IGEPAL CA-630 (Abcam)] and transferred to 96-well v-bottomed plates (Corning) and then centrifuged at 500 G for 5 min. The supernatant was removed with a multichannel pipette, and the nuclei pellets were resuspended in 50 μL of transposition buffer [25 μL 2× TD buffer (Illumina), 2.5 μL Tn5 transposase (Illumina), and 22.5 μL nuclease-free H_2O]. The Nextera XT DNA Library Preparation Kit supplied all Illumina transposition reagents. The plate was incubated at 37 °C on a shaker set to 800 rpm. Then, transposed DNA was purified using a Qiagen MinElute kit according to the manufacturer instructions and frozen at −80 °C.

Library generation. The following day, samples were thawed and amplified using PCR with Illumina TG Nextera® XT Index Kit v2 Set A to generate libraries of transposase-liberated fragments from each replicate (43). The reaction was monitored with qPCR to prevent GC bias and oversaturation. After PCR, the samples were again purified using the Qiagen MinElute kit and analyzed via the Agilent High-Sensitivity DNA Bioanalyzer. Samples were then stored at −80 °C. When the samples were ready to be sequenced, each sample was diluted to a final concentration of 20 nM and pooled for paired-end sequencing with a NovaSeq 6000 instrument on an S2 flowcell, using a 100 bp cassette. Two sequencing runs were performed, each time normalizing sample concentration and generating a final pool. Two replicates, β-glucan #2 and hydroquinone #3, were excluded from sequencing at this step due to low DNA yield.

ATAC-seq Analysis.

Raw ATAC-seq fastQ processing. All computation was performed on the University of Chicago's Midway3 Research Computing Cluster. FastQ sequencing outputs from two sequencing runs were concatenated using the cat command in Linux. Adapters were removed with NGmerge (Version 0.3), and bowtie2 (Version 2.5.1) aligned the resulting sequences to mouse index genome mm10, downloaded from bowtie2's manual (https://bowtie-bio.sourceforge.net/bowtie2/manual.shtml) on 2 May 2023 (44, 45) SAMtools (Version 1.13) sort, view, fixmate, and markdup were used to remove PCR duplicates, with SAMtools index and view used to remove mitochondrial sequences (46).

Quality control was performed with FastQC (Version 0.12.1) in Linux and with ATACseqQC (Version 1.16.0) in R (Version 4.1.0) (47).

ATAC-seq Peak Identification.

Calling peaks and identifying consensus peaks. Model-based analysis for ChIP-Seq (MACS2) callpeak (Version 2.2.7.1) in Python (Anaconda 2020.11) was used to distinguish any peaks from background observed in all samples (48). Peaks were called using the command for each replicate:

macs2 callpeak -f BAMPE -t <sampleN.sorted.bam> -g mm -n <sampleN> -B --keep-dup all

For our analysis, we used MACS2 with the default settings tailored for the Mus musculus genome (specified as -g mm). Our approach to estimating the expected background was as follows: We multiplied the number of reads by their length and then divided by the mappable genome size, which is the standard method used to analyze ATAC-seq data. This calculation assumes that in the absence of genuine peaks, reads would be evenly distributed throughout the genome. To be identified as a peak by MACS2, a region needs to show an enrichment of at least 10 times above this expected background.

Next, we removed blacklisted genes with BEDTools (Version 2.18) intersect -a (49). To generate a set of consensus peaks, we set our reference peakset for all samples to be the MACS2 output file with the most total peaks identified, which was beta glucan replicate #3 using the command bedtools intersect -wa -a. All replicates were each then intersected with our reference peakset to generate a consensus array of peaks applicable to all samples. Finally, a single count matrix of all reads within the region covered by each consensus peak for all replicates was made with the join command in Linux.

Differential Accessibility Analysis.

Step One: Limma (Version 3.48.3) (50). To format counts for modeling of differential accessibility in limma, we created a DGElist object and applied calcnormFactors with edgeR (Version 3.34.1) (51). Limma's voom function generated a normalized counts-per-million matrix. Two outliers generated an aberrant bimodal mean-variance trend in limma voom and principal component analysis with R's native *prcomp* function. These outliers, flunisolide replicate #3 and hydrocortisone #3, were removed from subsequent analysis.

For all remaining samples, peaks with low counts (consensus peaks with a median across treatments of counts-per-million less than 1) were filtered out from subsequent analysis. We used a design matrix of ~1 + molecule + processOrder in limma. processOrder corresponds to an ascending integer values based on the sequence of experimental sample processing–we modeled this effect as a linear effect of time on the quality of samples upon observation of spread in multidimensional space along the first two principal components of normalized consensus peak counts between PBS control replicates processed at the beginning of the plate (#1 to 3) versus at the end (#4 to 6).

Step Two: Mashr (Version 0.2.69) (28). In order to maximize power to identify differential accessibility regions, we applied a second modeling step to the limma-generated prior log fold changes, multivariate adaptive shrinkage (mash). The gain in power is derived from the fact that mash incorporates correlations in effect sizes among treatment conditions, under the assumption that some effects are likely to be shared. We determined that application of the data-driven covariance model (implemented according to the vignette accessed in September of 2023 at https://stephenslab.github.io/mashr/articles/intro_mash_dd.html) yielded increased log-likelihood score compared to modeling with the canonical covariance matrix. To correct for correlations in effects caused by using a single source of BMDMs across all treatments and replicates, we applied mashr's method which accounts for correlations among measurements (method one in vignette at https://stephenslab.github.io/mashr/articles/intro_correlations.html) in addition to the data-driven covariance matrix. The resulting posterior betas were used to identify peaks with statistically significant differences in accessibility between each treatment condition and the PBS control.

Two-List Gene Set Overenrichment Analysis.

Step one: Peak annotation. In order to determine whether differentially accessible chromatin peaks localized near genes with shared functional biological pathways, we first assigned peaks to genes using HOMER annotatePeaks.pl (52). We used HOMER version 4.11.1 with mouse accession and ontology version 6.3, mouse promoters version 5.5, and mouse genome and annotation version 6.4 from http://homer.ucsd.edu/homer/data accessed in September of 2023. Next, for each treatment condition, we filtered out duplicate peaks which mapped to the same gene, retaining only the gene peak with the strongest signal [highest product of the mashr posterior beta and local false sign rate (LFSR)]; this produced a list of peaks in which each gene annotation occurs only once.

Step two: Overenrichment analysis. From these lists, peaks with statistically significant (LFSR < 0.05) increases in chromatin accessibility compared to the PBS control were selected per treatment condition. The R package fgsea (Version 1.27.0) (53) provided the over-representation analysis (ORA) hypergeometric test used to determine overenrichment of genes represented in the list of peaks with increased accessibility in each experimental treatment compared to a second background, "gene universe" list of all consensus peaks detected, similarly filtered as in step one to include only one instance of each gene. Pathways queried with fgsea ORA were from the REACTOME database (54). Analysis was performed similarly to the vignette accessed in September of 2023, and the threshold for significance was set at P adjusted < 0.1 (55).

TF Motif Enrichment Analysis. We identified regions of chromatin with peaks of increased accessibility in each experimental treatment condition relative to PBS based on the mashr model results and then applied HOMER's findMotifsGenome.pl software to determine whether sequence motifs associated with binding of specific TFs were associated with any of these regions of increased accessibility.

TF Footprinting Analysis. First, we merged replicate bam format files (preprocessed as described above in *Raw ATAC-seq fastQ processing* for each treatment condition with Samtools merge such that each treatment condition had one bam file. Next, we called peaks on the merged bam files using the command:

macs2 callpeak -f BAMPE -t <sample>.bam -g mm -n ./<sample> -B --keep -dup all

On these peak sets, we called footprints using HINT-ATAC from the Regulatory Genomics Toolbox (56). *P* value adjustment was performed using the Benjamini–Hochberg correction via the *P*.adjust function in R. JASPAR database motifs were obtained using the MotifDb and ggseqlogo packages in R (57–59).

Statistical Analysis and Data Representation. Statistical analysis on in vitro and in vivo datasets was performed using GraphPad Prism (v8). Data were analyzed using one- or two-way ANOVA with multiple comparisons. Direct comparisons were made using the 1-tailed or 2-tailed Student's *t* test. Data are reported as mean ± SD. The number of replicates is reported in the figure descriptions. For in vitro experiments, n represents the number of technical replicates, while for in vivo or ex vivo experiments, n represents the number of animals. Figures were produced with GraphPad Prism, BioRender, R, ChemDraw, and Adobe Illustrator.

Data, Materials, and Software Availability. ATAC sequencing data have been deposited in GEO (GSE270608) (60).

ACKNOWLEDGMENTS. We thank Anna Slezak for manuscript edits; Zander Galluppi for viability processing advice; Raul Aguirre Gamboa and Sarah Sun for programming advice and examples; and Matthew Stephens and Yuxin Zao for mashr modeling advice. H.R.K. is funded by the NSF Graduate Research Fellowship Program: award NSF 2140001. This work was supported by the National Institute of Allergy and Infectious Diseases of the NIH under the Discovery of Adjuvant Program: award NIH 75N93019C00041 and the Defense Threat Reduction Agency award HDTRA11810052 to A.E.-K. The work was also supported by grant R01-GM134376 to L.B., and the UChicago DDRCC, Center for Interdisciplinary Study of Inflammatory Intestinal Disorders (C-IID) (NIDDK P30 DK042086). We would also like to thank the Cellular Screening Center (CSC), Genomics Facility, and Animal Resources Center (ARC) at the University of Chicago for their excellent support of this work.

1. M. G. Netea *et al.*, Defining trained immunity and its role in health and disease. *Nat. Rev. Immunol.* **20**, 375–388 (2020).
2. R. J. W. Arts *et al.*, Glutaminolysis and fumarate accumulation integrate immunometabolic and epigenetic programs in trained immunity. *Cell Metab.* **24**, 807–819 (2016).
3. M. G. Netea, R. van Crevel, BCG-induced protection: Effects on innate immune memory. *Semin. Immunol.* **26**, 512–517 (2014).
4. P. Aaby *et al.*, Randomized trial of BCG vaccination at birth to low-birth-weight children: Beneficial nonspecific effects in the neonatal period? *J. Infect. Dis.* **204**, 245–252 (2011).
5. S. Bekkering *et al.*, In vitro experimental model of trained innate immunity in human primary monocytes. *Clin. Vaccine Immunol.* **23**, 926–933 (2016).
6. J. Kleinnijenhuis *et al.*, Bacille Calmette-Guérin induces NOD2-dependent nonspecific protection from reinfection via epigenetic reprogramming of monocytes. *Proc. Natl. Acad. Sci. U.S.A.* **109**, 17537–17542 (2012).
7. S.-C. Cheng *et al.*, mTOR- and HIF-1 -mediated aerobic glycolysis as metabolic basis for trained immunity. *Science* **345**, 1250684–1250684 (2014).
8. C. D. C. C. van der Heijden *et al.*, Aldosterone induces trained immunity: The role of fatty acid synthesis. *Cardiovasc. Res.* **116**, 317–328 (2020).
9. C. D. C. C. van der Heijden *et al.*, Catecholamines induce trained immunity in monocytes in vitro and in vivo. *Circ. Res.* **127**, 269–283 (2020).
10. L. Edgar *et al.*, Hyperglycemia induces trained immunity in macrophages and their precursors and promotes atherosclerosis. *Circulation* **144**, 961–982 (2021).
11. L. A. Groh *et al.*, oxLDL-induced trained immunity is dependent on mitochondrial metabolic reprogramming. *Immunometabolism* **3**, e210025 (2021).
12. J. Ajit *et al.*, Novel non-immunogenic trained immunity inducing small molecule with improved anti-tumor properties. bioXriv [Preprint] (2024). https://doi.org/10.1101/2024.03.22.585780v1 (Accessed 28 March 2024).
13. O. N. F. King *et al.*, Quantitative high-throughput screening identifies 8-hydroxyquinolines as cell-active histone demethylase inhibitors. *PLoS One* **5**, e15535 (2010).
14. J. Li *et al.*, A high-throughput screening campaign against PFKFB3 identified potential inhibitors with novel scaffolds. *Acta Pharmacol. Sin.* **44**, 680–692 (2023).
15. L. Sartori *et al.*, Thieno[3,2-b]pyrrole-5-carboxamides as new reversible inhibitors of histone lysine demethylase KDM1A/LSD1. Part 1: High-throughput screening and preliminary exploration. *J. Med. Chem.* **60**, 1673–1692 (2017).
16. Y. Zhou *et al.*, Development of novel human lactate dehydrogenase A inhibitors: High-throughput screening, synthesis, and biological evaluations. *Eur. J. Med. Chem.* **177**, 105–115 (2019).
17. S. Fanucchi, J. Domínguez-Andrés, L. A. B. Joosten, M. G. Netea, M. M. Mhlanga, The intersection of epigenetics and metabolism in trained immunity. *Immunity* **54**, 32–43 (2021).
18. A. Ziogas, M. Bruno, R. van der Meel, W. J. M. Mulder, M. G. Netea, Trained immunity: Target for prophylaxis and therapy. *Cell Host Microbe* **31**, 1776–1791 (2023).
19. R. M. Eglen, A. Gilchrist, T. Reisine, The use of immortalized cell lines in GPCR screening: The good, bad and ugly. *Comb. Chem. High Throughput Screen.* **11**, 560–565 (2008).
20. P. Saz-Leal *et al.*, Targeting SHIP-1 in myeloid cells enhances trained immunity and boosts response to infection. *Cell Rep.* **25**, 1118–1126 (2018).
21. J. Y. Kim *et al.*, Discovery of new states of immunomodulation for vaccine adjuvants via high throughput screening: Expanding innate responses to PRRs. *ACS Cent. Sci.* **9**, 427–439 (2023), 10.1021/acscentsci.2c01351.
22. S. T. Johnston, E. T. Shah, L. K. Chopin, D. L. Sean McElwain, M. J. Simpson, Estimating cell diffusivity and cell proliferation rate by interpreting IncuCyte ZOOMTM assay data using the Fisher-Kolmogorov model. *BMC Syst. Biol.* **9**, 38 (2015).
23. J. Ajit *et al.*, Temporal control of trained immunity via encapsulated release of β-Glucan improves therapeutic applications. *Adv. Healthc. Mater.* **11**, 2200819 (2022).
24. D. Cruz-Topete, J. A. Cidlowski, One hormone, two actions: Anti- and pro-inflammatory effects of glucocorticoids. *Neuroimmunomodulation* **22**, 20–32 (2014).
25. S. F. Sorrells, R. M. Sapolsky, An inflammatory review of glucocorticoid actions in the CNS. *Brain Behav. Immun.* **21**, 259–272 (2007).
26. A. E. Barber *et al.*, Glucocorticoid therapy alters hormonal and cytokine responses to endotoxin in man. *J. Immunol.* **150**, 1999–2006 (1993).
27. S. Bekkering *et al.*, Oxidized low-density lipoprotein induces long-term proinflammatory cytokine production and foam cell formation via epigenetic reprogramming of monocytes. *Arterioscler. Thromb. Vasc. Biol.* **34**, 1731–1738 (2014).
28. S. M. Urbut, G. Wang, P. Carbonetto, M. Stephens, Flexible statistical methods for estimating and testing effects in genomic studies with multiple conditions. *Nat. Genet.* **51**, 187–195 (2019).
29. K. Baidžajevas *et al.*, Macrophage polarisation associated with atherosclerosis differentially affects their capacity to handle lipids. *Atherosclerosis* **305**, 10–18 (2020).
30. L. Yang *et al.*, Diagnostic and prognostic value of autophagy-related key genes in sepsis and potential correlation with immune cell signatures. *Front. Cell Dev. Biol.* **11**, 1218379 (2023).
31. S. B. Larsen *et al.*, Establishment, maintenance, and recall of inflammatory memory. *Cell Stem Cell* **28**, 1758–1774.e8 (2021).
32. A. R. Black, J. D. Black, J. Azizkhan-Clifford, Sp1 and krüppel-like factor family of transcription factors in cell growth regulation and cancer. *J. Cell. Physiol.* **188**, 143–160 (2001).
33. Y. Yuan *et al.*, The transcription factor KLF14 regulates macrophage glycolysis and immune function by inhibiting HK2 in sepsis. *Cell. Mol. Immunol.* **19**, 504–515 (2022).
34. M. D. Ilsley *et al.*, Krüppel-like factors compete for promoters and enhancers to fine-tune transcription. *Nucleic Acids Res.* **45**, 6572–6588 (2017).
35. E. Ciarlo *et al.*, Trained immunity confers broad-spectrum protection against bacterial infections. *J. Infect. Dis.* **222**, 1869–1881 (2020).
36. J. Ajit *et al.*, β-glucan induced trained immunity enhances antibody levels in a vaccination model in mice. bioRxiv [Preprint] (2024), https://doi.org/10.1101/2024.04.11.588932 (Accessed 17 April 2024).
37. C. Ding *et al.*, Inducing trained immunity in pro-metastatic macrophages to control tumor metastasis. *Nat. Immunol.* **24**, 239–254 (2023).
38. G.C.-F. Chan, W. K. Chan, D.M.-Y. Sze, The effects of β-glucan on human immune and cancer cells. *J. Hematol. Oncol. J. Hematol. Oncol.* **2**, 25 (2009).
39. A. C. Hesseling *et al.*, The risk of disseminated Bacille Calmette-Guerin (BCG) disease in HIV-infected children. *Vaccine* **25**, 14–18 (2007).
40. S. Norouzi, A. Aghamohammadi, S. Mamishi, S. D. Rosenzweig, N. Rezaei, Bacillus Calmette-Guérin (BCG) complications associated with primary immunodeficiency diseases. *J. Infect.* **64**, 543–554 (2012).
41. M. G. Netea, J. W. M. van der Meer, Trained immunity: An ancient way of remembering. *Cell Host Microbe* **21**, 297–300 (2017).
42. W. J. M. Mulder, J. Ochando, L. A. B. Joosten, Z. A. Fayad, M. G. Netea, Therapeutic targeting of trained immunity. *Nat. Rev. Drug Discov.* **18**, 553–566 (2019).
43. J. Buenrostro, B. Wu, H. Chang, W. Greenleaf, ATAC-seq: A method for assaying chromatin accessibility genome-wide. *Curr. Protoc. Mol. Biol.* **109**, 21.29.1–21.29.9 (2015).
44. J. M. Gaspar, NGmerge: Merging paired-end reads via novel empirically-derived models of sequencing errors. *BMC Bioinformatics.* **19**, 536 (2018).
45. B. Langmead, S. L. Salzberg, Fast gapped-read alignment with Bowtie 2. *Nat. Methods* **9**, 357–359 (2012).
46. P. Danecek *et al.*, Twelve years of SAMtools and BCFtools. *GigaScience* **10**, giab008 (2021).
47. E. G. Wilbanks, M. T. Facciotti, Evaluation of algorithm performance in ChIP-Seq peak detection. *PLoS One* **5**, e11471 (2010).
48. Y. Zhang *et al.*, Model-based analysis of ChIP-Seq (MACS). *Genome Biol.* **9**, R137 (2008).
49. A. R. Quinlan, I. M. Hall, BEDTools: A flexible suite of utilities for comparing genomic features. *Bioinformatics.* **26**, 841–842 (2010).
50. M. E. Ritchie *et al.*, limma powers differential expression analyses for RNA-sequencing and microarray studies. *Nucleic Acids Res.* **43**, e47 (2015).
51. M. D. Robinson, D. J. McCarthy, G. K. Smyth, edgeR: A Bioconductor package for differential expression analysis of digital gene expression data. *Bioinformatics.* **26**, 139–140 (2010).
52. S. Heinz *et al.*, Simple combinations of lineage-determining transcription factors prime cis-regulatory elements required for macrophage and B cell identities. *Mol. Cell* **38**, 576–589 (2010).
53. G. Korotkevich *et al.*, Fast gene set enrichment analysis. bioXriv [Preprint] (2021). https://doi.org/10.1101/060012 (Accessed 1 June 2023).
54. M. Gillespie *et al.*, The reactome pathway knowledgebase 2022. *Nucleic Acids Res.* **50**, D687–D692 (2022).
55. T. Sagendorf, 8.2 over-representation analysis | PRoteomics data analysis in R/bioconductor. https://pnnl-comp-mass-spec.github.io/proteomics-data-analysis-tutorial/ora.html (Accessed 1 October 2023).
56. Z. Li *et al.*, Identification of transcription factor binding sites using ATAC-seq. *Genome Biol.* **20**, 45 (2019).
57. P. Shannon, M. Richards, MotifDb: An annotated collection of protein-dna binding sequence motifs version 1.32.0 from bioconductor. (2023). https://rdrr.io/bioc/MotifDb/ (Accessed 1 June 2023).
58. O. Wagih, ggseqlogo: A versatile R package for drawing sequence logos. *Bioinformatics* **33**, 3645–3647 (2017).
59. A. Sandelin, W. Alkema, P. Engström, W. W. Wasserman, B. Lenhard, JASPAR: An open-access database for eukaryotic transcription factor binding profiles. *Nucleic Acids Res.* **32**, D91–D94 (2004).
60. E. Ketter, Data from "High-throughput screen identifies non inflammatory small molecule inducers of trained immunity." GEO. https://www.ncbi.nlm.nih.gov/geo/query/acc.cgi?acc=GSE270608. Deposited 24 June 2024.